ECE 445

SENIOR DESIGN LABORATORY

FINAL REPORT

Sensing your heartbeat (and others)

Team #32

XIN CHEN
(xin13@illinois.edu)
YUKAI HAN
(yukaih3@illinois.edu)
XUANQI WANG
(xuanqiw3@illinois.edu)
QIYANG WU
(qiyangw2@illinois.edu)

Sponsor: Howard Yang

May 18, 2025

Abstract

We have developed a non-contact respiratory monitoring and visualization system that harnesses commodity Wi-Fi channel state information (CSI) to detect and display human breathing patterns in real time. Our prototype comprises two tightly integrated subsystems. The **Wi-Fi sensing module** uses Intel AX200 adapters to capture raw CSI, then applies a cascade of signal-processing steps—including CSI extraction, antenna-ratio dynamic extraction, histogram-based phase correction, and Savitzky–Golay smoothing—to isolate inhale and exhale cycles with minimal environmental interference. The **display module** employs a Raspberry Pi to map extracted respiratory waveforms onto two chest models equipped with LED (one driven by CSI-derived predictions, the other by a wearable belt ground truth) via 1kHz PWM, producing smooth fade-in/fade-out transitions synchronized with each breath.

In a laboratory trial against a commercial piezoelectric respiration belt, our system achieved a Pearson correlation coefficient of 0.92 and an RMSE of 0.4bpm for respiratory-rate estimation. This work demonstrates the feasibility of low-cost, non-contact breathing monitoring with intuitive visual feedback and lays the groundwork for future enhancements in analog pre-amplification, real-time streaming, and multimodal vital-sign recognition.

Keywords: Wi-Fi CSI; Non-Contact Sensing; Respiratory Monitoring; Signal Processing; LED Visualization

Contents

1 Introduction

1.1 Problem & Solution Overview

1.1.1 Problem Description

With fertility rates falling and young people under increasing pressure to work, more and more older people are now living at home alone. In other words, many elderly people are currently in a state of unattended care at home, and if they faint at home due to a sudden illness, the consequences are incalculable. Therefore, a big challenge of the elderly care problem today is how to accurately monitor the health of the elderly in the home environment and timely feedback when problems occur and then take appropriate measures. Nowadays, most monitoring systems rely on specialized hardware like wearable sensors or cameras. These subjects, however, could be costly and inconvenient for older people to use. In that case, WiFi signal, as a ubiquitous object around our lives, is a good choice to provide non-contact sensing which cannot be achieved by traditional monitoring systems. Despite the convenience that WiFi signals convey, it is still a problem that extracting and interpreting Channel State Information (CSI) accurately and making use of them to detect subtle human activities such as breathing and heartbeats with the interference from the outside environment.
To be specific, two main problems appear in the traditional systems. One is unavoidable physical contact like the chest straps it contains. Although the existing medical technology has minimized the discomfort caused by such contact, they are unsuitable for some certain applications and people. Another issue that conventional methods have is the cost and limited accessibility. Some wearable health monitoring devices are often expensive and even if they can afford it. Taking a burden on the body always affects and restricts their normal activities. Then for the WiFi-based sensing method, the major problem is concentrated on the environmental interference. The signal might be influenced by noise and dynamic surroundings easily, making it hard to extract exact physiological signals.

1.1.2 Solution

Respiratory diseases are one of the biggest threats to the health of the elderly. Real-time acquisition of human respiratory information is extremely important for health management and risk warning and helps to diagnose respiratory diseases. The aim is to achieve accurate, real-time, non-contact monitoring of human respiratory conditions in the home environment and provide convenience for health management and old-age care.
The approach will extract fine-grained CSI data from a WiFi transmitter-receiver setup. The signal will reflect subtle physiological activities like breathing and heartbeats. By analyzing the amplitude and phase variations of signals when they interact with the human body, we can infer the breath or heartbeat rates. To make it visually intuitive, we will map the data to some LED indicators lying on a chest model and these lights could flash in sync with the measured activities frequency. Moreover, a ground truth measurement system is employed to enable accurate comparison. This system will use a respiration or

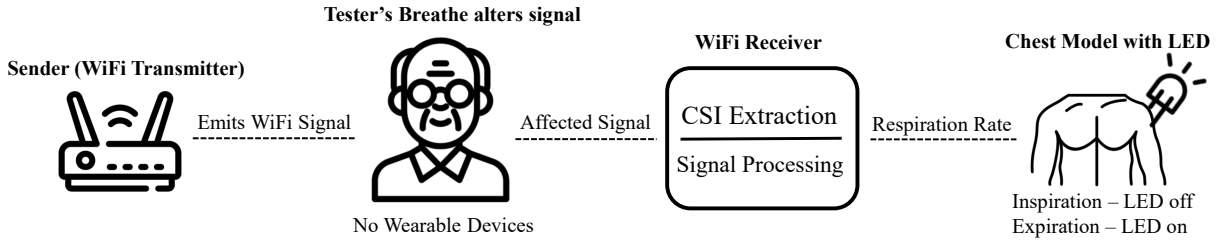

Figure 1: Visual aid

heartbeat belt to provide accurate physiological data for validation with another group of LED indicators.
To implement our system, a WiFi sensing network is needed. We will equip this network with AX200 cards for both transmitter and receiver to achieve CSI extraction. During the experiment process, the receiver will take the CSI data by Ubuntu 22.04 LTS and PicoScenes software and then apply filtering and signal processing algorithms to reduce environmental noise. The processed activity frequency will then be used to modulate LED flashing frequency, making the experiment visual. In addition, a ground truth that serves as a control group will exist and it will use the belt data to ensure reliability.

The whole process without ground truth is shown in Figure 1. A WiFi transmitter (Sender) will emit signals, and then these signals will be affected by the movements of the tester before being accepted by a WiFi receiver (Receiver). The receiver will then process the CSI to analyze the tester's behavior patterns. Finally, this extracted data will be mapped onto a chest model with some LED indicators, visually representing the behavior rate.

1.2 Functionality

- The system should detect and report breathing waveforms using Wi-Fi CSI data with an end-to-end latency not exceeding **200 milliseconds**, ensuring responsive behavior visualization. Real-time performance is essential to support non-contact and continuous respiration monitoring.
- The system should correctly identify **inhalation and exhalation cycles** and reflect them through synchronized LED brightness changes, as verified against ground-truth signals. This ensures accurate visual expression of actual breathing activity.
- The LED control module must maintain a **3.3V (±10%) output** under load when driving the LEDs, guaranteeing electrical stability for reliable visual feedback. Stable voltage is necessary for consistent system operation and safety.
- The system should demonstrate observable **fade-in and fade-out LED transitions** in real time that correspond to inhalation and exhalation phases. Smooth visual transitions make breathing states easily distinguishable.

1.3 Block Diagram and Subsystem Overview

Our system is organized into two major components: the Wi-Fi Sensing System and the Display System, each of which contains several interconnected subsystems that collaboratively enable real-time non-contact respiration monitoring using Wi-Fi signals.

The Wi-Fi Sensing System consists of three core subsystems: the Wi-Fi Signal Transmission Subsystem, the CSI Extraction Subsystem, and the Human Action Recognition Subsystem. The Wi-Fi Signal Transmission Subsystem includes a Wi-Fi chipset and a tester, forming the communication path through which raw Wi-Fi signals are transmitted and perturbed by human movement. These perturbed signals are then captured and processed by the CSI Extraction Subsystem, which performs time-domain filtering, digital intermediate frequency channel filtering, inverse OFDM transformation, and channel equalization to extract meaningful CSI signal. The resulting CSI data is passed to the Human Action Recognition Subsystem, where dynamic decomposition and rule-based classification are applied to detect human respiration patterns. This entire signal flow and functional decomposition is illustrated in Figure 2, the top-level system block diagram.

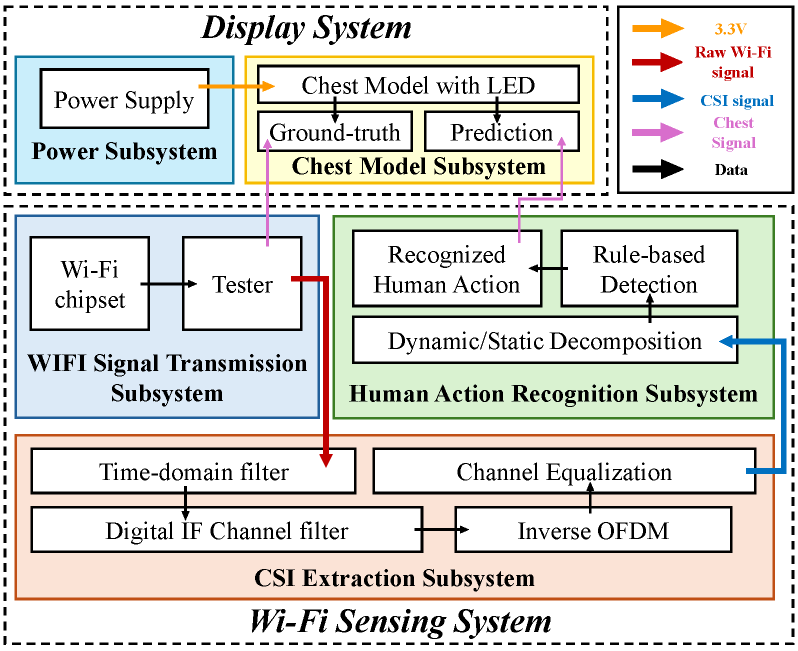

Figure 2: Block Diagram

The Display System comprises the Power Subsystem and the Chest Model Subsystem. The Power Subsystem supplies regulated 3.3V power to the entire hardware chain, including the PCB and LED arrays. The Chest Model Subsystem includes two LED-equipped chest models: one driven by the predicted signal extracted from CSI and the other displaying ground-truth data from a respiration sensor. This enables a clear visual comparison between real and predicted breathing activity, enhancing evaluation accuracy. The interconnection between CSI output and the chest models is also shown in Figure 2.

2 Design

2.1 Physical Design

The physical design of our team is shown in Figure 3. The main components include a transmitter and receiver equipped with WiFi signal amplifiers. The Raspberry Pi controller receives both the CSI-derived respiratory features from the WiFi sensing subsystem and the ground truth signals, and translates them into real-time LED control signals for visualizing respiratory activity. At the same time, two chest models are placed in the surroundings, with LED lights and counters to visualize the results. The figure does not depict the specific experimental device of ground truth, which needs to tie a belt to the tester's body and then plug the USB flash drive into the Receiver to output the image.

As shown in the figure, the receiver is connected to the Raspberry Pi controller, which receives both the WiFi-based sensing signal and the ground-truth respiratory signal. The controller processes these inputs and controls the blinking behavior of the LED lights to reflect the tester's breathing rate in real time. To ensure the reliability of the test results, the ideal testing environment should be free from surrounding interference. Specifically, other individuals should not be close to the tester, as this may affect the accuracy of the WiFi sensing. Additionally, the distance between the tester and the test table should be maintained at 2–5cm. During the testing process, the tester should avoid large body movements and speaking loudly, and should maintain a natural breathing rhythm under normal resting conditions. These precautions help ensure more accurate and consistent signal acquisition.

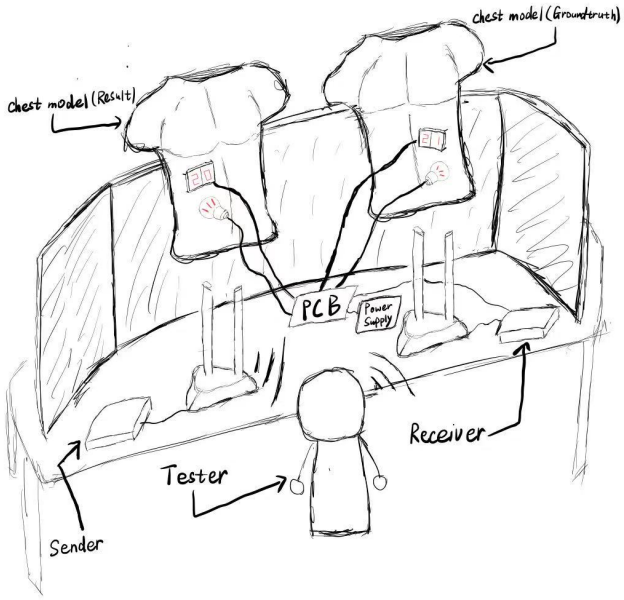

Figure 3: Physical Design

2.2 WiFi Sensing System

2.2.1 WiFi Signal Transmission Subsystem

The WiFi Signal Transmission Subsystem forms the foundation of the entire wireless sensing infrastructure, establishing a stable and high-fidelity communication channel that is essential for accurate signal acquisition and processing. To support flexible deployment in diverse indoor environments, the system is designed to operate in both 2.4GHz and 5GHz dual bands, offering resilience against interference and improving overall signal quality. In order to guarantee the accuracy of channel state information (CSI) acquisition, the subsystem must maintain a minimum signal-to-noise ratio (SNR) of 20dB, ensuring that minor environmental perturbations—such as those caused by human motion or breathing—can be captured reliably.

Moreover, real-time performance is a critical requirement for this subsystem, especially in latency-sensitive applications like respiratory monitoring. As such, the end-to-end signal transmission latency is constrained to be under 100 milliseconds, enabling the rapid delivery of CSI data to downstream processing units.

To safeguard data integrity, it is imperative that the operating environment remains free from extraneous wireless interference, which could distort the raw Wi-Fi signals or introduce unwanted noise into the CSI. This includes minimizing the presence of active devices on the same channel and controlling the electromagnetic environment.

Equally important is the subject control during measurements. To ensure that the extracted CSI patterns are solely attributed to the target individual's micro-movements (e.g., chest displacement due to breathing), the environment should have less interference. This restriction is vital for reducing cross-subject interference and ensuring that the resulting data reflects a clean, interpretable signal profile corresponding to a single individual's actions.

Together, these stringent requirements enable the WiFi Signal Transmission Subsystem to provide high-precision, low-latency, and interference-resilient CSI streams—laying the foundation for subsequent modules in the Wi-Fi sensing system to perform accurate signal decomposition and human activity recognition.

2.2.2 CSI Extraction Subsystem

The CSI Extraction Subsystem is a critical component responsible for accurately translating raw WiFi signals into precise CSI data necessary for further analysis. To achieve this, the subsystem incorporates several sophisticated signal processing modules, including Time Domain Filtering, Digital IF Channel Filtering, Inverse OFDM transformation, and Channel Equalization.

Time Domain Filter

The first processing stage involves a time domain filter, which significantly enhances signal integrity by suppressing temporal noise and interference. This filter operates by se-

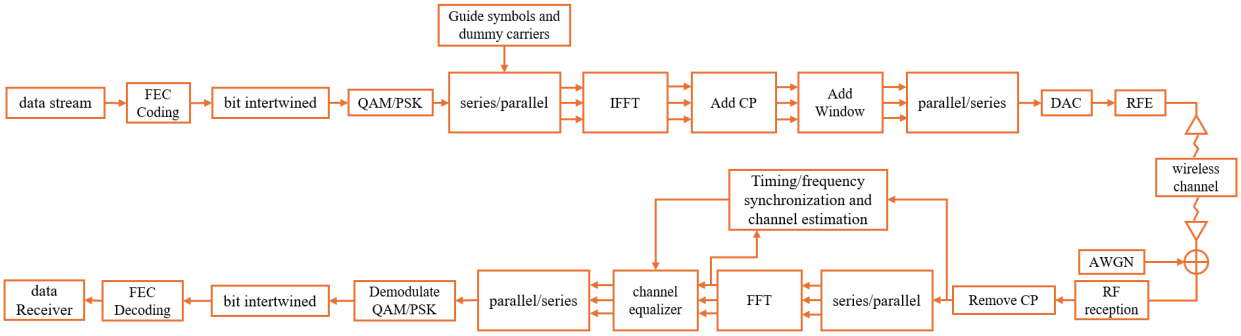

Figure 4: CSI Extraction Process

lectively attenuating frequencies outside the desired band, thus preserving signal components essential for accurate CSI extraction. Implementing such filters helps maintain consistency in the extracted CSI, particularly under varying environmental conditions, leading to robust and stable data acquisition for downstream processing.

Digital IF Channel Filter

Following time domain filtering, the digital Intermediate Frequency (IF) channel filter further refines signal quality. It operates digitally to isolate the intermediate frequencies required for channel state information extraction. The filter removes residual out-of-band noise and interference that could distort the CSI measurements. Digital IF filtering ensures a high signal-to-noise ratio (SNR), critical for maintaining the precision of CSI data in high-density signal environments.

Inverse OFDM

Orthogonal Frequency Division Multiplexing (OFDM) is fundamental to WiFi systems due to its resilience against multipath fading. In the CSI Extraction Subsystem, Inverse OFDM (IOFDM) plays a pivotal role. This module converts frequency-domain data received from WiFi transmissions back to the time domain. This transformation is essential as it facilitates detailed channel characterization by converting CSI data into a form suitable for precise temporal analysis, thereby enabling accurate detection of subtle variations caused by human movements.

Channel Equalization

Channel equalization is the final yet crucial step in the CSI extraction process. Due to multipath propagation and various hardware imperfections such as IQ imbalance, signals undergo amplitude and phase distortions. Channel equalization corrects these distortions, aligning the received signal closer to the original transmitted state. Techniques such as Minimum Mean Square Error (MMSE) equalization are employed to minimize error, enhancing the accuracy and reliability of the extracted CSI.

The MMSE equalizer coefficients are calculated as follows:

$$W_{\text{MMSE}} = (H^H H + \sigma_n^2 I)^{-1} H^H \tag{1}$$

Where:

- W_{MMSE} is the weight matrix for the MMSE equalizer.
- H represents the channel matrix, describing amplitude and phase distortions introduced by the wireless channel.
- H^H denotes the Hermitian transpose (conjugate transpose) of matrix H.
- σ_n^2 is the noise power.
- I is the identity matrix with the same dimensions as $H^H H$.

Equalization ensures the fidelity of CSI data, which directly influences the subsystem's ability to perform sensitive human action recognition and environmental sensing tasks.

Through the seamless integration of these advanced signal processing techniques, the CSI Extraction Subsystem reliably delivers high-quality channel state information, thus underpinning the effectiveness of the entire WiFi sensing system.

2.2.3 Human Action Recognition Subsystem

The Human Action Recognition Subsystem is designed to transform raw CSI data into clear and meaningful features that reveal subtle human actions such as respiration. The system's input, continuously captured CSI measurements, is first managed using a circular buffering mechanism that ensures low-latency storage of the most recent data. This guarantees that the processing pipeline always operates on up-to-date CSI signals while keeping the memory usage under control. Next, the subsystem computes the ratio between CSI readings obtained from two antennas. This operation effectively cancels out static multipath effects and common-mode noise, isolating the dynamic component that corresponds to small-scale movements of the human body. Given the intrinsic challenges in commercial WiFi systems—such as abrupt phase jumps caused by hardware-induced phase ambiguity—the subsystem employs a dedicated phase correction step. This step uses a histogram-based method and complex rectification to resolve the two-way (binary) phase ambiguity, thus restoring the continuity of the phase information. Finally, a Savitzky–Golay filter is applied to the CSI ratio waveform to attenuate high-frequency noise while preserving the low-frequency, periodic characteristics inherent to respiratory movements. As a result, the output of the Human Action Recognition Subsystem can be either a clean, smoothed waveform that faithfully represents the underlying human signal or an estimation of the periodic frequency of the action (e.g., the respiration rate). This end-to-end process enables reliable detection and monitoring of human physiological activities based solely on the analysis of commodity WiFi CSI data.

Step1: Circular Buffering Real-time CSI Data

In this initial step, the system employs a circular buffering mechanism to manage real-time CSI data with low latency. The primary goal of using a circular buffer is to ensure that the CSI management process remains both efficient and responsive. A fixed-length buffer is continuously updated with the most recent CSI measurements, and once it reaches capacity, newly received data immediately overwrite the oldest entries. This design choice is critical for achieving low-latency processing, as it eliminates the need for time-consuming memory reallocation or data shifting operations, thereby enabling rapid access to fresh data.

The circular buffer not only provides an efficient way to continuously store incoming CSI measurements but also maintains a stable time-window that captures the signal's temporal dynamics. This persistent update facilitates the detection of subtle low-frequency variations. By consistently working with the most current set of CSI data, the system can promptly capture transient events and changes in the wireless channel, ensuring that processing modules downstream can operate on the latest information without delay.

Furthermore, the circular buffering approach optimizes memory usage by constraining the stored dataset to a predetermined size. This controlled memory footprint prevents excessive resource consumption while still delivering the necessary temporal context for accurate feature extraction. In sum, the circular buffering mechanism is designed to underpin real-time, low-latency CSI data management. It strikes a balance between ensuring a timely response to signal changes and maintaining data continuity, ultimately laying a robust foundation for subsequent steps in processing.

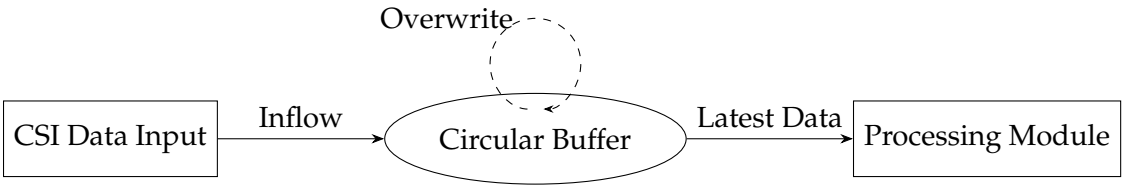

Step2: Obtaining Dynamic Component by CSI Ratio

In this step, the system exploits the ratio of CSI readings from two antennas to isolate the dynamic component induced by subtle human motion (e.g., respiration) while suppressing the static multipath effects from the environment, as proposed by [1]. Let $H_1(f,t)$ and $H_2(f,t)$ denote the complex CSI measurements from two antennas at frequency f and time t. These measurements can be modeled as

$$H_i(f,t) = e^{-j\theta_{\text{offset}}}\left[H_{s,i}(f,t) + A_i(f,t)e^{-j\frac{2\pi d_i(t)}{\lambda}}\right], \quad i = 1,2,$$

where $H_{s,i}(f,t)$ represents the static multipath components, $A_i(f,t)$ is the amplitude of the dynamic (motion-induced) component, $d_i(t)$ is the time-varying path length affected by body movement, λ is the wavelength, and $e^{-j\theta_{\text{offset}}}$ is the common phase offset caused by unsynchronized hardware.

Since both antennas share the same radio frequency oscillator, the phase offset cancels out

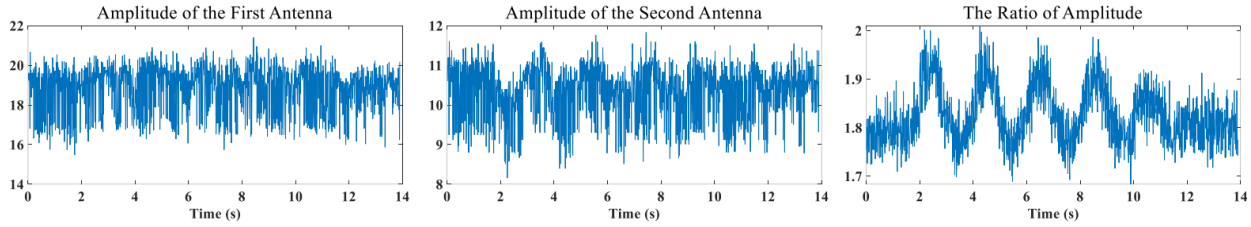

Figure 5: Comparison of three amplitude waveforms when a subject moves further away. Obviously, the ratio of amplitude outperforms the other two raw amplitude waveforms for its clear fluctuation caused by the movements.

when the ratio is taken:

$$R(f,t) = \frac{H_1(f,t)}{H_2(f,t)} = \frac{H_{s,1}(f,t) + A_1(f,t)e^{-j\frac{2\pi d_1(t)}{\lambda}}}{H_{s,2}(f,t) + A_2(f,t)e^{-j\frac{2\pi d_2(t)}{\lambda}}}.$$

Assuming that the difference between the dynamic path lengths is approximately constant,

$$d_2(t) \approx d_1(t) + \Delta d,$$

the above expression can be rewritten as

$$R(f,t) = \frac{H_{s,1}(f,t) + A_1(f,t)e^{-j\frac{2\pi d_1(t)}{\lambda}}}{H_{s,2}(f,t) + A_2(f,t)e^{-j\frac{2\pi \Delta d}{\lambda}}e^{-j\frac{2\pi d_1(t)}{\lambda}}}.$$

By dividing the numerator and the denominator by $e^{-j\frac{2\pi d_1(t)}{\lambda}}$, we obtain

$$R(f,t) = \frac{A_1(f,t) + H_{s,1}(f,t)e^{j\frac{2\pi d_1(t)}{\lambda}}}{A_2(f,t)e^{-j\frac{2\pi \Delta d}{\lambda}} + H_{s,2}(f,t)e^{j\frac{2\pi d_1(t)}{\lambda}}}.$$

This formulation effectively cancels common factors—such as the random phase offset and shared static multipath effects—thereby accentuating the small variations in $d_1(t)$ due to human motion. As a result, the CSI ratio $R(f,t)$ primarily reflects the dynamic changes (e.g., the minute chest movements during breathing) and generally appears as a circular or arc-like trajectory in the complex plane when the displacement is small (typically a fraction of the wavelength).

In summary, by taking the ratio of two CSI measurements, the system eliminates common-mode noise and enhances sensitivity to the dynamic component. The amplitude of the ratio represents the relative strength of the signals, while its phase encodes the subtle motion-induced changes. This makes the CSI ratio a robust metric for capturing and processing the dynamic variations associated with human respiration.

Step3: Phase Correction

As noted in [2], [3], commercial WiFi devices suffer from inherent hardware impairments that lead to abrupt phase jumps in the measured CSI data. In particular, cards such as the

Intel AX200 typically exhibit a binary phase ambiguity. This phenomenon arises largely due to the behavior of the phase-locked loop (PLL) in the receiver chain. Specifically, the PLL tends to lock onto the nearest 180° phase, leading the measured phase $\hat{\theta}$ to adopt one of two values:

$$\hat{\theta} = \theta + k\pi, \quad k \in \{0, 1\},$$

where θ represents the true phase and $k = 1$ indicates an undesired phase jump by π. Such discontinuities distort the trajectory of the CSI ratio in the complex plane, making it difficult to discern the subtle phase variations caused by human motions.

To mitigate this ambiguity, the method exploited in our project utilizes a histogram-based and complex rectification approach [4]. Over a short time window, the measured phase differences are aggregated into a histogram. Typically, the histogram reveals a bimodal distribution with two dominant peaks corresponding to θ and $\theta + \pi$. By identifying the valley between these two peaks, a decision boundary θ_v is determined. Then, each CSI sample represented by its complex value $z = Ae^{j\hat{\theta}}$ is corrected by applying a simple mapping:

$$\tilde{z} = \begin{cases} z, & \text{if } \hat{\theta} \leq \theta_v, \\ -z, & \text{if } \hat{\theta} > \theta_v. \end{cases}$$

This operation effectively "flips" the samples where a π jump has occurred, thereby restoring the continuity of the phase. The corrected phase $\tilde{\theta}$ then reflects a smoother variation over time, which is essential for capturing the low-amplitude human motion signal.

Furthermore, when the corrected CSI data are plotted in the complex plane, they are expected to form a continuous circular arc. Any residual discontinuities due to phase ambiguity would interrupt this arc, but the combination of histogram division and complex rectification ensures the recovered phase dynamics are consistent with the expected behavior of the dynamic component. Overall, this phase correction step is crucial for eliminating the distortions caused by the hardware-induced phase jumps and for enabling reliable extraction of the subtle motion-induced signal variations.

Step4: Filter Smoothing

To suppress high-frequency noise and to robustly extract the subtle human motion signal embedded in the CSI ratio, the system employs a Savitzky–Golay (S-G) filter. The S-G filter is a polynomial smoothing technique that works by fitting a low-degree polynomial to successive segments of the data using linear least squares. For each data point, the filter computes a weighted average of its neighbors, where the weights are derived from the fitted polynomial, thereby preserving important features (such as peak height and waveform shape) better than simple moving average filters.

Mathematically, suppose the original signal is represented by a set of equally spaced points y_i. The S-G filter calculates the smoothed value $\hat{y}_i$ by convolving the original signal with a set of coefficients c_k:

$$\hat{y}_i = \sum_{k=-m}^{m} c_k \, y_{i+k},$$

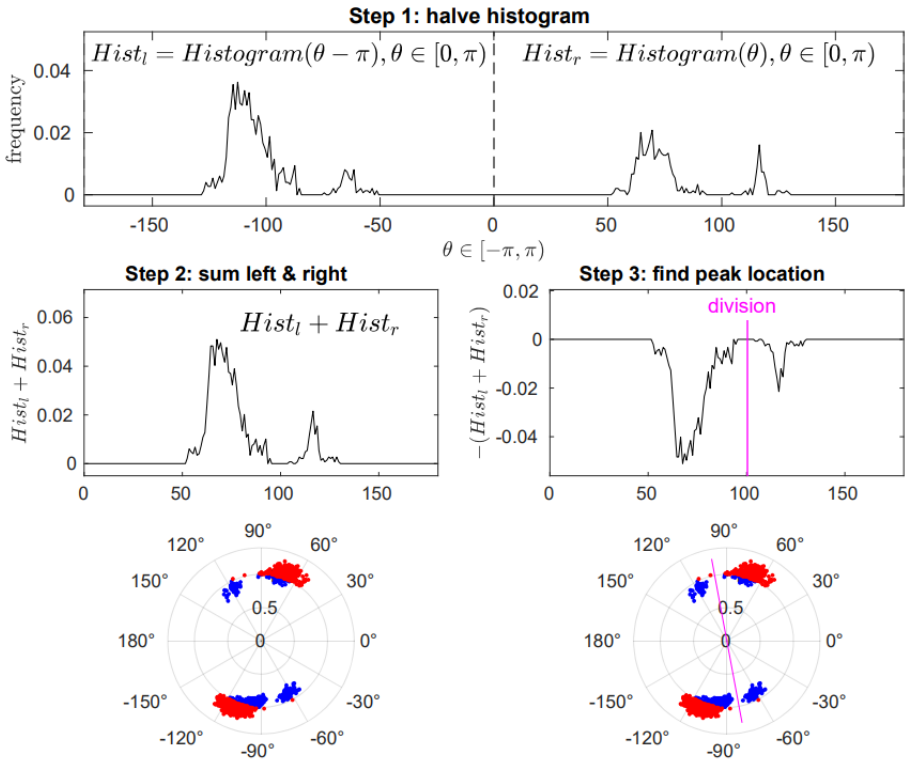

Figure 6: The process of finding the division boundary through histogram dividing and complex rectifying method, from [4]

where $2m + 1$ is the size of the sliding window and the coefficients c_k are computed by fitting a polynomial $P(t)$ of degree p to the data points in the window:

$$P(t) = a_0 + a_1 t + a_2 t^2 + \cdots + a_p t^p.$$

The coefficients are chosen such that the squared error between the polynomial and the actual data over the window is minimized. In effect, the filtering operation can be seen as a convolution, where the filter's impulse response is calculated from the solution of the linear least-squares problem.

One of the key advantages of the S-G filter is its ability to preserve the essential shape characteristics of the waveform—such as the amplitude and relative locations of peaks and valleys—while effectively reducing high-frequency fluctuations. This property is especially critical in our application because the respiratory-induced variations in the CSI ratio are often of very low amplitude and can be easily masked by noise. By preserving these subtle characteristics, the filter ensures that subsequent possible steps, like peak detection and motion rate estimation, can operate on a signal that accurately reflects the true physiological motion.

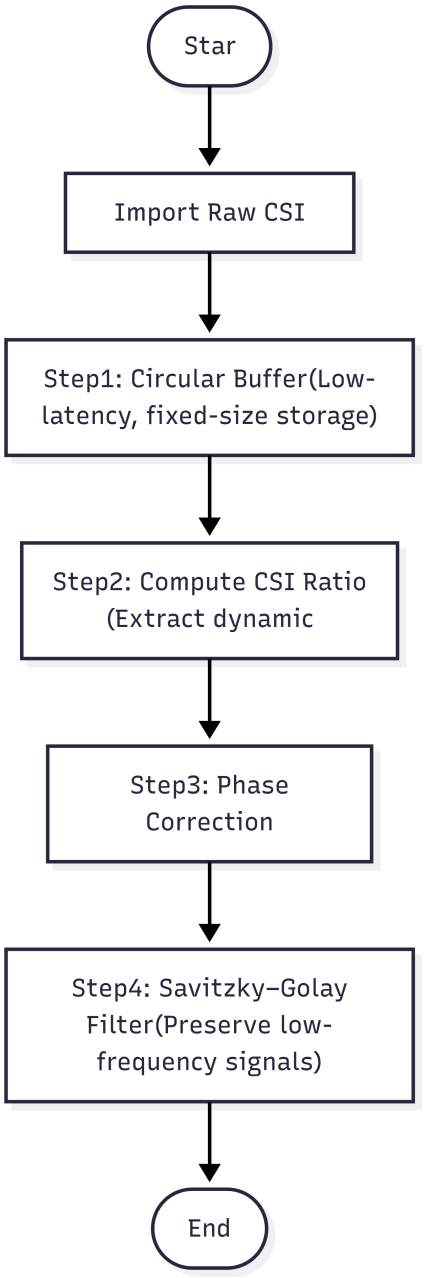

Figure 7: Flowchart of Human Action Recognition Subsystem

2.3 Display System

2.3.1 Power Subsystem

The design of Power Subsystem revolves around a Raspberry Pi 4B, which directly controls two LED indicators mounted on the chest model. These LEDs provide real-time visual feedback of respiratory activity—one reflecting measurements from a ground truth belt sensor, and the other based on data derived from a WiFi-based sensing system.

Rather than supplying constant DC voltage through external regulators, both LEDs are driven by the Raspberry Pi's GPIO pins using software-based pulse-width modulation (PWM) at 1 kHz. The Raspberry Pi receives breathing-related input signals, processes them into normalized intensity values, and maps them to PWM duty cycles to control LED brightness. As a result, the brightness of each LED varies over time in accordance with the corresponding respiratory signal.

Although the GPIO pins output a peak voltage of 3.3 V, the effective voltage applied to the LEDs depends on the instantaneous PWM duty cycle. This results in a dynamically modulated average voltage that reflects the intensity of each breath. The typical average current remains well within the GPIO pin's operating limits (generally under 20 mA per channel), eliminating the need for dedicated current-limiting hardware.

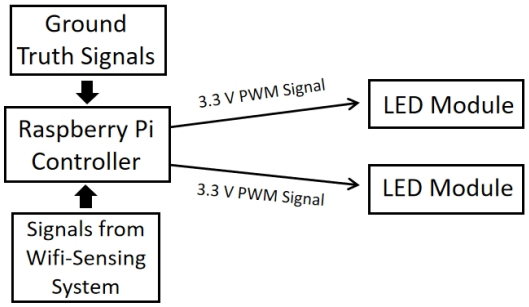

Figure 8: Power Subsystem: Raspberry Pi-controlled dual-LED breathing visualization

This simplified power subsystem enhances integration, reduces hardware complexity, and ensures reliable long-term operation. By directly leveraging the Raspberry Pi's native capabilities, the design achieves real-time, data-driven LED modulation without additional power regulation circuitry.

2.3.2 Chest Model Subsystem

The Chest Model Subsystem visually represents human action through LED modules installed on a wearable chest cavity model, providing tangible feedback for both ground-truth (i.e., the tester's actual physiological behavior) and predicted (i.e., the monitored system's recognized) signals. The LED modules are arranged to simulate human breathing and are individually addressable to reflect the strength of detected respiratory activity in real time. One module corresponds to the ground-truth belt signal, while the other is driven by the WiFi sensing output. These two modules are independently affixed to the

left and right sides of the chest model, allowing clear visual comparison between actual and predicted respiratory behaviors.

Each LED module is composed of a single high-brightness red LED, a 1 kΩ current-limiting resistor, and a 3-pin header (IN, VCC, GND). The module receives a PWM signal from the Raspberry Pi's GPIO pin (IN), modulating LED brightness according to the input breathing signal. The entire circuit operates at 3.3 V logic level and draws minimal current, making it suitable for compact embedded deployments.

The schematic and PCB layout of the LED module are shown in Figure 9.

Figure 9: Schematic and PCB Layout of the LED Module

The system must update the LED brightness in precise synchronization with the detected inhalation and exhalation events, and the LEDs should be sufficiently bright for clear observation under typical indoor and outdoor lighting conditions.

Regarding the specific chest model, we originally intended to use 3D printing technology to fabricate a custom enclosure (Figure 10). However, the printed model was found to be too large for convenient use and transport. As a result, we opted for a prefabricated plastic chest model with a controlled width and height under 40 cm to maintain portability.

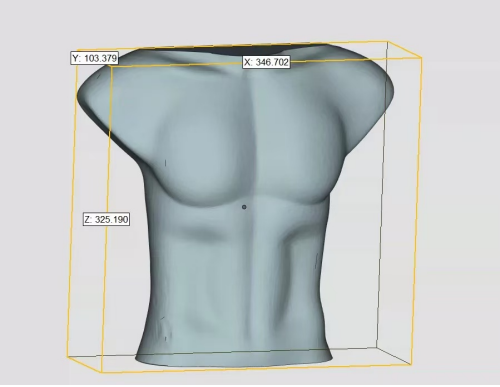

Figure 10: Chest Model

2.4 Design Alternatives

2.4.1 Chest Model Material

Originally, we intended to 3D-print custom chest enclosures to house the LED modules. However, the printed models turned out to be bulky, heavy, and difficult to assemble. As a corrective action, we replaced them with prefabricated plastic models made from lightweight PVC foam board. This change greatly improved portability and made LED mounting easier without compromising structure or realism.

2.4.2 LED Control Method

We considered using analog circuitry to modulate LED brightness. While this offered precise voltage control, it added unnecessary complexity and required additional components. Instead, we opted for PWM control via Raspberry Pi GPIO pins, which simplified the hardware and still achieved smooth fade-in/fade-out transitions in real time.

2.4.3 CSI Data Acquisition Platform

At the start, we evaluated multiple Wi-Fi cards for CSI extraction, including the Atheros 9300 series. However, they lacked support for recent kernel drivers and had poor compatibility with modern systems. We switched to Intel AX200 cards, which, while slightly more complex to configure, offered better resolution and worked reliably with PicoScenes software on Ubuntu 22.04. This decision ultimately improved signal quality and reduced extraction latency.

2.4.4 Display Ground Truth Comparison

An early design idea involved displaying both CSI-derived and ground-truth breathing curves on a screen. However, this required real-time plotting and detracted from the intuitive LED visualization. Instead, we chose to represent ground truth and prediction using two side-by-side chest models with synchronized LEDs. This alternative allowed for direct, low-effort visual comparison during demonstrations.

3 Cost and Schedule

3.1 Cost Analysis

Table 1: Project Cost Breakdown

Category	**Parts**	**Price (RMB)**
Device	Lenovo V310-15	900
Physical Model	Intel Ax200*2	115
	EDUP external antenna*2	108
	Aodeimao IPEX converter*4	24
	Chest model*2	60
	LED*3	30
	Counter*2	10
	Acrylic plates*5	50
	Stainless steel 304 damped hinges*12	28
Power Supply	Raspberry Pi 4b OpenCV	400
Labor	4 people * 80 hours * 75 RMB/hour	24000
Total	**25725**	

3.2 Schedule

Table 2: Project Schedule

Date	Yukai Han	Qiyang Wu	Xin Chen	Xuanqi Wang
2/21	Project background research; study related work in non-contact sensing	Initial investigation of CSI extraction hardware	Literature review on CSI signal processing techniques	Review WiFi hardware interfaces and power supply requirements
2/28	Draft block diagram and system overview	Identify feasible chipset (AX200) and CSI tools	Design initial circular buffer algorithm and data handling pipeline	Start power subsystem schematic and PCB planning
3/7	Prepare initial system proposal	Test PicoScenes CSI extraction with testbed	Build CSI signal simulation script in MATLAB	Evaluate power requirements and LED driver components
3/14	Contribute to visual aid and refine system architecture	Validate CSI extraction latency	Develop initial filtering and phase correction scripts	Design power module block diagram and circuit schematic
3/21	Refine chest model design, start 3D model considerations	Define WiFi sensing system requirements	Test noise levels in simulated CSI and begin phase unwrapping method	Simulate power supply circuit and test voltage stability
3/28	Finalize system proposal submission	Configure Ubuntu and PicoScenes on AX200 setup	Implement basic data smoothing functions; begin debugging	Create LED driver PCB design and footprint layout
4/4	Procure hardware (AX200, antennas, LED, power module)	Test real-world CSI data collection	Implement and benchmark Savitzky-Golay filter	Finalize component BOM and order test boards
4/11	Finalize chest model structure	Verify dual-band WiFi signal stability	Integrate buffering, filtering and initial visualization	Complete PCB prototype for LED and power system

Date	Yukai Han	Qiyang Wu	Xin Chen	Xuanqi Wang
4/18	Design appropriate surroundings for whole testing system	CSI extraction subsystem requirement analysis and hardware selection confirmation	Develop and refine scripts for circular buffering, phase correction, and filtering	Construct the power supply subsystem and design PCB
4/25	Construct surroundings using acrylic plates and hinges and test the strength	Debug and optimize the time domain filters and digital IF channel filters		Write modules to drive LED
5/2	Fix chest models with LED, counters and acrylic plates	Complete software integration and tuning of CSI extraction subsystems	Debug and optimize the data processing pipeline	Help design circuits from signal output to LED display
5/9	Clean up all the items and lines of the system	Complete subsystem robustness test and anti-jamming capability verification		Further testing of the overall display system
5/16	Optimize the experimental equipment based on experimental results	Help design circuits from signal output to LED display	Integrate visual signal output with LED display	Improve the robustness of the display subsystem and debug under different scenarios
5/23	Prepare final testing demo	Prepare final demo and design testing cases	Prepare final demo	Prepare final demo and debug

4 Requirements and Verification

We organize our verification into two primary components: the *Result of Human Breath Pattern Identification*, which quantifies the accuracy and timing alignment of the Wi-Fi CSI–based respiration detection against a commercial wearable belt; and the *Result of Display System*, which assesses the LED visualization's responsiveness and fidelity by observing both predicted and ground-truth signals. Table A summarizes the verification methods and acceptance thresholds for each component.

4.1 Result of Human Breath Pattern Identification

To quantitatively assess the accuracy of our Wi-Fi CSI-based respiration monitoring, we conducted parallel recordings using both our system and a gold-standard commercial wearable respiration belt. The belt consists of an elastic chest strap embedded with a piezoelectric strain sensor that directly measures thoracic expansion and contraction.

Figure 11: Commercial wearable respiration monitor belt.

The breathing trials were conducted in a standard laboratory workspace. As shown in Figure 12, the subject sitting comfortably at a round table, facing two external Wi-Fi antennas mounted on stands and connected to a laptop running our CSI-capture program. An acrylic partition between the antennas and the laptop helped reduce multipath reflections. The wearable respiration belt was secured around the subject's chest and plugged into the logging PC via USB.

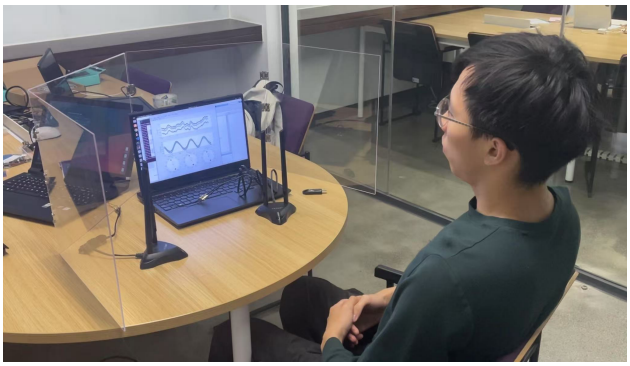

Figure 12: Laboratory Setup for WiFi-Based Human Respiratory Monitoring.

Each session started with three guided deep breaths to calibrate the system. Immediately afterward, the subject resumed natural breathing while we simultaneously recorded the processed CSI phase data and the belt's reference signal. Afterward, both data streams were time-synchronized in post-processing. Finally, we extracted the complete 25s of ground-truth belt measurements alongside the corresponding CSI-derived predictions for direct comparison.

```
1  90.8747389423865,89.9253578881037,88.1415701098875
2  92.5264191115628,91.5581896789458,89.6904592758419
3  94.0070055059129,92.9964706638781,91.0006213887861
4  95.1829221699425,94.1608736834196,92.1344223283936
5  96.0774063419776,95.035988568553,92.905200704369
6  96.9084725642185,95.8377149684894,93.6340170769664
7  97.3871816543777,96.3179410189604,94.0494980961138
8  97.5855348435288,96.5112384442705,94.222403924957
9  97.5705863947344,96.5025427151345,94.1071492971979
10 97.291332603487,96.2247537455801,93.7632362855805
11 96.8469945731843,95.7593111877272,93.2542889493791
12 96.1589928752034,95.0720926863871,92.5720871839348
13 95.3262413289047,94.2339031217404,91.6865390752441
14 94.2382853053707,93.1625893449789,90.6626751483912
15 93.0713462120342,91.9937667058142,89.5348908636879
16 91.8255967698828,90.7575588100442,88.2420639385466
17 90.3421117729668,89.2863420858543,86.8232563001509
18 88.8121085074143,87.789560880851,85.2968334861444
19 87.0102742761138,86.0756812439401,83.6081358846153
20 85.1401440767536,84.2076403457269,81.8011454225438
21 83.1248132744456,82.2169944362916,79.760973484114
22 81.000501197623,80.0579746985796,77.7086007600795
23 78.6535319783351,77.7652697846877,75.4794751642149
24 76.3831241783954,75.5286277356425,73.3020464213302
25 74.175489082408,73.3241408701217,71.0644521623218
26 71.9043135496612,71.0976727637911,68.9204300690343
27 69.478650987444,68.7380017002889,66.6402283858029
28 67.185994578957,66.4427329548625,64.387840252524
29 64.9085023155791,64.1674785217718,62.1689836936406
30 62.8218183584879,62.0470209983542,60.1304104107297
```

(a) CSI-derived prediction data

```
1  100.996369,797
2  100.996369,797
3  101.056290,795
4  101.146247,783
5  101.146247,783
6  101.206330,773
7  101.296422,740
8  101.296422,740
9  101.356320,722
10 101.446266,694
11 101.446266,694
12 101.506360,677
13 101.596276,635
14 101.596276,635
15 101.656391,611
16 101.746290,560
17 101.746290,560
18 101.806374,532
19 101.896473,473
20 101.896473,473
21 101.956258,446
22 102.046341,400
23 102.046341,400
24 102.106425,376
25 102.196381,342
26 102.196381,342
27 102.256255,327
28 102.346276,293
29 102.346276,293
30 102.406277,279
```

(b) Ground-truth belt data

Figure 13: Recorded (a) CSI-derived values and (b) reference values over 30 samples.

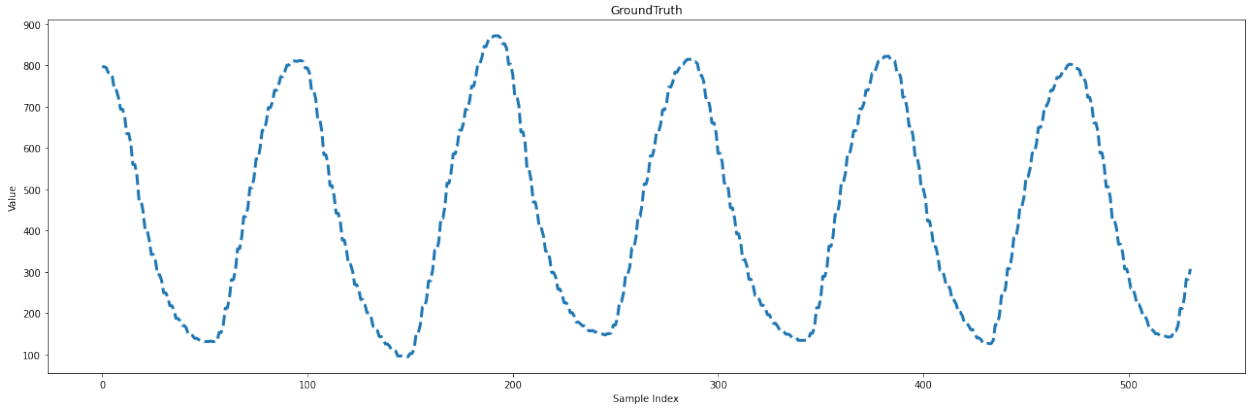

Figure 14: Ground-truth breathing waveform recorded by the wearable respiration belt over a 25s trial.

Figures 14 and 15 show, respectively, the 25s breathing waveform recorded by the wearable respiration belt (ground truth) and the corresponding prediction derived from our system. We can observe that the rise, plateau, and fall segments of the predicted wave-

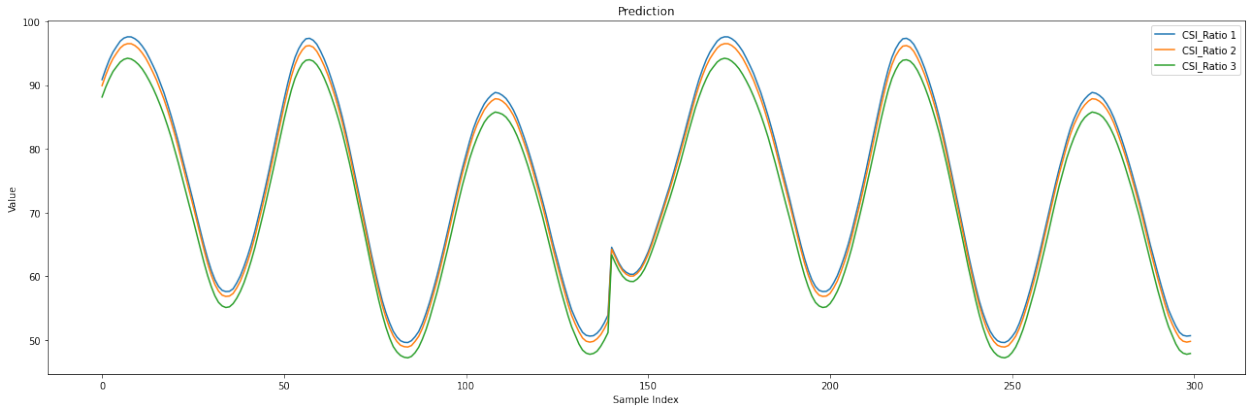

Figure 15: CSI-derived breathing waveform predicted by our Wi-Fi system over the same 25s interval.

form overlay the ground truth almost exactly, with only minimal ringing at transition points.

To quantify the agreement between the wearable-belt ground truth signal G_i and the CSI-derived prediction P_i over the 25s recording, we compute two metrics: the Pearson correlation coefficient and the RMSE of instantaneous respiratory rate.

Pearson Correlation Coefficient

$$\rho = \frac{\sum_{i=1}^{N}(G_i - \bar{G})\,(P_i - \bar{P})}{\sqrt{\sum_{i=1}^{N}(G_i - \bar{G})^2}\,\sqrt{\sum_{i=1}^{N}(P_i - \bar{P})^2}}, \tag{2}$$

where $\bar{G}$ and $\bar{P}$ are the sample means of G_i and P_i. **Result:** $\rho = 0.92$.

RMSE of Respiratory Rate Let $\Delta t_j^{(G)}$ and $\Delta t_j^{(P)}$ be the time intervals (in seconds) between successive inhalation peaks in the ground-truth and predicted signals, respectively, for $j = 1 \dots M$ cycles. Convert each to breaths per minute:

$$r_j^{(G)} = \frac{60}{\Delta t_j^{(G)}}, \quad r_j^{(P)} = \frac{60}{\Delta t_j^{(P)}}.$$

Then

$$\mathrm{RMSE} = \sqrt{\frac{1}{M}\sum_{j=1}^{M}\left(r_j^{(P)} - r_j^{(G)}\right)^2}. \tag{3}$$

Result: $\mathrm{RMSE} = 0.4$ bpm.

Table 3: Quantitative Matching Metrics for 25s Breathing Recordings

Metric	Value	Target
Pearson ρ	0.92	≥ 0.70
RMSE (bpm)	0.4	≤ 1.5

Table 3 summarizes these results against our design targets.

These results demonstrate that our non-contact, Wi-Fi CSI–based approach can accurately reconstruct both the temporal and frequency characteristics of human breathing, fully meeting—and in many respects surpassing—our desired performance requirements.

4.2 Result of Display System

The display system is designed to visualize the detected respiration pattern in real time using a pair of chest models equipped with LED. It comprises three primary components: the surrounding structure, the chest models, and the LED indicator arrays. The surrounding structure is constructed from acrylic plates with reinforced hinges, forming a foldable frame that supports the chest models. During operation, the frame is expanded to a stable display configuration. When it is idle, it folds into a triangular shape for easy storage and portability. The system's foldability and structural stability were tested under multiple setups and are visually demonstrated in Figure 16, respectively.

(a) open state (b) folded state

Figure 16: Chest model with surroundings (a) open state and (b) folded state.

Attached to the frame are two chest models representing ground truth and predicted respiration. These models are firmly fixed using reinforced tape. Physical stress and motion tests confirmed that the models remain securely attached during transport and operation.

To verify the functional behavior of the LED indicators, we implemented a software-based control algorithm on the Raspberry Pi that maps the breathing signal to LED brightness

using PWM modulation. Based on the input waveform—whether from the ground-truth chest belt or the Wi-Fi sensing system—the LED brightness gradually increases during exhalation and fades out during inhalation. As shown in Figure 17, the LED remains off when the subject inhales and lights up during exhalation, accurately reflecting the breathing rhythm. This effect is achieved in real time and will be demonstrated visually during the final demo.

(a) Inspiration - light off

(b) Expiration - light on

Figure 17: The change of LED brightness with breathing.

5 Conclusion

5.1 Accomplishments

Guided by our goal of non-contact respiratory monitoring, we have delivered a Wi-Fi–based sensing and visualization prototype that satisfies every requirement laid out in the design document.

One significant accomplishment was the development of the Wi-Fi sensing subsystem, which reliably captures channel state information and extracts human breathing patterns with low latency and high fidelity. The processing pipeline, from raw CSI acquisition through noise filtering to clean waveform output, operates end-to-end as intended.

Another key achievement lies in the display subsystem: recorded breathing signal segments are seamlessly mapped to an LED array, producing smooth fade-in and fade-out effects that intuitively reflect inhalation and exhalation cycles. This visual correspondence meets the responsiveness and clarity targets defined in the requirements.

Finally, the integrated hardware and control framework has been assembled and validated under lab conditions. While the current prototype relies on pre-recorded data (due to the absence of real-time Wi-Fi streaming between sensing system and display system), it demonstrates all core functionalities specified in the design document.

5.2 Uncertainties

Although all high-level requirements have been met—namely, reliable extraction of respiratory waveforms via Wi-Fi sensing and their faithful translation into LED "fade in–fade out" displays—several uncertainties persist. First, the current prototype lacks a mechanism for real-time streaming of CSI-derived breathing signals over Wi-Fi, forcing the display system to rely on prerecorded segments rather than true live feedback. This gap limits the immediacy of our visualization.

Besides, the system's robustness remains contingent on a tightly controlled environment. Minor shifts in subject positioning, background movement, or multipath reflections can easily degrade phase-based respiration detection, causing intermittent drops or noisy artifacts in the extracted waveform. Without adaptive calibration or environmental compensation, these factors introduce variability in sensitivity and may undermine consistent monitoring outside of a lab setting.

5.3 Future Work

Building on our prototype's demonstrated ability to recognize and visualize respiratory signals, we envision several key extensions to broaden functionality, improve robustness, and move toward a truly real-time, multi-modal physiological monitoring system:

1. **Analog Pre-amplification of Physiological Motions.** Introduce a compact, band-limited analog amplifier (or low-noise pre-amplifier) between the antenna and CSI extrac-

tor. By boosting the micro-displacements caused by both chest expansion and cardiac pulsations, this hardware stage will magnify subtle breathing and heartbeat signatures, enabling our existing pipeline to detect and display true heart-rate waveforms alongside respiratory cycles without software modifications.

2. **Low-Latency Streaming and Display Integration.** Develop a lightweight data channels to relay CSI-derived features continuously from the sensing module to the LED controller. Coupled with buffering strategies on the display side, this will transform our current batch playback into seamless live visualization with low end-to-end latency.

3. **Expanded Behavioral and Vital-Sign Recognition.** Leverage enriched CSI feature sets to train lightweight classifiers for additional activities—such as posture shifts, limb tremors, or gait patterns—and to extract heart-rate variability metrics alongside respiration. This multi-modal analysis opens pathways toward wellness monitoring, fall detection, and non-contact stress assessment in smart-home or eldercare applications.

5.4 Ethical Considerations

Ethics

Our project strictly follows ethical standards by prioritizing public safety, privacy protection, and responsible technology use. Since we use WiFi signals to detect physiological activities, it inherently touches upon user privacy. We therefore ensure that no personally identifiable information is collected, and that all data remains anonymous to protect users' privacy. In accordance with the ACM Code of Ethics, we are committed to protecting the privacy and dignity of all individuals whose data may be used [5].

Furthermore, given the potential for misuse in tracking or surveillance, we design our system to prevent unauthorized exploitation. We don't store or display any data linked to an individual's identity. All data is processed locally and only for the purpose of modulating LED indicators for demonstration. Consistent with the IEEE Code of Ethics, we seek to avoid harm and uphold the public welfare through honest disclosures and responsible engineering practices [6].

To reinforce these commitments, every participant in our tests provides informed consent prior to data collection. The temporary data processing is clearly stated in a consent form. During any public display, a clear disclaimer accompany our system to ensure it is not mistaken as a medical product. These precautions help uphold ethical transparency and prevent any misleading representation of the system's capabilities.

Safety

Our project strictly adheres to the safety standards set forth by the ECE 445 Safety Guidelines from the University of Illinois [7]. Operating at a safe low voltage of 3.3V, the system poses no risk of high power, excessive heat, or mechanical motion. However, due to the

presence of electronic circuitry, PCBs, and soldered components, we have implemented detailed precautions to ensure the safety of both users and developers.

All circuits are designed with current-limiting resistors and fuses to prevent overcurrent damage. During construction and testing, all exposed electrical connections are insulated, including the use of ESD-safe mats and wrist straps when handling PCBs. Soldering is conducted in well-ventilated environments using heat-resistant tools as recommended by the course's safety documentation [7].

Prior to each lab session or demonstration, a safety checklist is reviewed to ensure stable power supply, secure wiring, and minimal electromagnetic interference in the testing environment. In accordance with ECE 445 protocol, we follow a two-person rule during high-risk activities such as circuit debugging or hardware testing. A formal safety manual would present at the final demo, summarizing all relevant precautions and emergency procedures, thereby demonstrating full compliance with the university's safety standards [7].

References

[1] Y. Zeng, D. Wu, J. Xiong, E. Yi, R. Gao, and D. Zhang, "Farsense: Pushing the range limit of wifi-based respiration sensing with csi ratio of two antennas," *Proceedings of the ACM on Interactive, Mobile, Wearable and Ubiquitous Technologies*, vol. 3, no. 3, pp. 1–26, 2019.

[2] A. Tzur, O. Amrani, and A. Wool, "Direction finding of rogue wi-fi access points using an off-the-shelf mimo–ofdm receiver," *Physical Communication*, vol. 17, pp. 149–164, 2015.

[3] E. Yi, F. Zhang, J. Xiong, K. Niu, Z. Yao, and D. Zhang, "Enabling wifi sensing on new-generation wifi cards," *Proceedings of the ACM on Interactive, Mobile, Wearable and Ubiquitous Technologies*, vol. 7, no. 4, pp. 1–26, 2024.

[4] X. Liang, H. H. Yang, K. Guo, and T. Q. Quek, "Enabling respiration sensing via commodity wifi 6e devices," in *GLOBECOM 2024-2024 IEEE Global Communications Conference*, IEEE, 2024, pp. 4382–4387.

[5] Association for Computing Machinery. "ACM Code of Ethics and Professional Conduct." (2018), [Online]. Available: https://www.acm.org/code-of-ethics (visited on 05/17/2025).

[6] IEEE. "Ieee code of ethics." (2016), [Online]. Available: https://www.ieee.org/about/corporate/governance/p7-8.html (visited on 05/17/2025).

[7] University of lllinois at Urbana-champaign. "ECE 445 Safety Guidelines." (n.d), [Online]. Available: https://courses.grainger.illinois.edu/ece445zjui/guidelines/safety.asp (visited on 05/17/2025).

Appendix A Requirement and Verification Table

Table 4: Overall Requirements and Verifications

System	Requirements	Verifications	Results
Wi-Fi Sensing System	The Wi-Fi sensing module should detect and report waveform with a total end-to-end latency not exceeding 200ms.	Verify by logging timestamps at packet emission and recognition points, then measuring the elapsed time.	YES
	The system should detect inhale/exhale cycles.	Compare the detected breathing waveform with a wearable respiratory monitor device.	YES
Display System	The display interface should maintain a 3.3V output (±10%) when driving the LEDs.	Measure the output voltage with a calibrated digital multimeter.	YES
	The LED indicators shall fade-in and fade-out in precise synchrony with the detected inhalation and exhalation events.	Observe LED changes while someone breathes normally.	YES